JACS
JOURNAL OF THE AMERICAN CHEMICAL SOCIETY

ARTICLE

pubs.acs.org/JACS

Gas-Bubble Effects on the Formation of Colloidal Iron Oxide Nanocrystals

Jared Lynch, Jiaqi Zhuang, Tie Wang, Derek LaMontagne, Huimeng Wu, and Y. Charles Cao*

Department of Chemistry, University of Florida, Gainesville, Florida 32611, United States

Supporting Information

ABSTRACT: This paper reports that gas bubbles can be used to tailor the kinetics of the nucleation and growth of inorganic-nanocrystals in a colloidal synthesis. We conducted a mechanistic study of the synthesis of colloidal iron oxide nanocrystals using gas bubbles generated by boiling solvents or artificial Ar bubbling. We identified that bubbling effects take place through absorbing local latent heat released from the exothermic reactions involved in the nucleation and growth of iron oxide nanocrystals. Our results show that gas bubbles display a stronger effect on the nucleation of iron oxide nanocrystals than on their growth. These results indicate that the nucleation and growth of iron oxide nanocrystals may rely on different types of chemical reactions between the iron−oleate decomposition products: the nucleation relies on the strongly exothermic, multiple-bond formation reactions, whereas the growth of iron oxide nanocrystals may primarily depend upon single-bond formation reactions. The identification of exothermic reactions is further consistent with our results in the synthesis of iron oxide nanocrystals with boiling solvents at reaction temperatures ranging from 290 to 365 °C, by which we determined the reaction enthalpy in the nucleation of iron oxide nanocrystals to be −142 ± 12 kJ/mol. Moreover, our results suggest that a prerequisite for effectively suppressing secondary nucleation in a colloidal synthesis is that the primary nucleation must produce a critical amount of nuclei, and this finding is important for *a priori* design of colloidal synthesis of monodispersed nanocrystals in general.

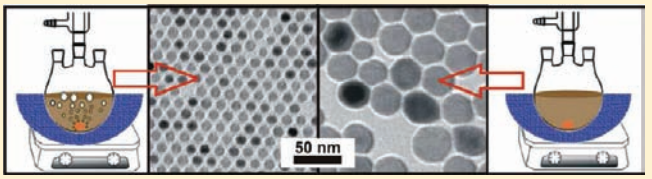

INTRODUCTION

The formation of gas bubbles absorbing the heat of vaporization from surrounding environments is an ordinary phenomenon in a boiling solvent under reflux.[1,2] In chemistry, reflux is a widely used technique to supply energy to chemical reactions, which can promote heat transfer and maintain reaction temperature in a narrow range; the solvent bubbles from the constant boiling action also serve to continuously mix the reaction solutions.[3] Here, we report that the formation of gas bubbles can significantly facilitate the nucleation of iron oxide nanocrystals in a solution-phase synthesis.

In the past two decades, exciting advances have been made in the synthesis of colloidal inorganic nanocrystals.[4] Two general synthetic approaches have been developed: one approach utilizes a rapid precursor injection into a hot growth solution,[5,6] and the other is a noninjection synthesis (NIS) in which the solution of reaction precursors is heated continuously to an elevated synthesis temperature.[7−10] The successful applications of these two types of syntheses have led to the preparation of a wide variety of high-quality nanocrystals with well-controlled size, shape, and composition.[4] The shape of these high-quality nanocrystals includes spheres, as well as nonspherical structures such as cubes, plates, prisms, and rods.[4,11] The composition of these nanocrystals includes metals, metal oxides, and the group II-VI and III-V semiconductors.[12] These monodispersed inorganic nanocrystals have enabled systematic elucidation of scaling laws of matter such as size-dependent semiconductor band gap, radiative rate, solid−solid phase transition pressure, superparamagnetic transition temperature, and surface plasmon resonance frequency.[13−18]

To date, kinetics studies have been extensively performed to explore the mechanisms of the nucleation and growth of monodispersed nanocrystals with nearly all available compositions.[5,19−21] Several molecular mechanisms of precursor evolution in colloidal syntheses have been revealed. For example, Alivisatos and co-workers found that the cleavage reaction of trialkylphosphine chalcogenides with an activation energy of 62.0 ± 2.8 kJ·mol^{-1} is important to the formation of group II-VI semiconductor nanocrystals.[20] However, it still remains a major challenge to bridge the molecular mechanisms of precursor evolution with the mechanisms of nanocrystal nucleation and growth. Most of the results from the studies of nanocrystal formation kinetics were only explained phenomenologically on the basis of classical nucleation theory and the LaMer diagram.[22]

The establishment of classical nucleation theory is based on the liquid-drop model and the Gibbs-Thompson equation, and this theory argues that the supersaturation of an "active monomer" is the driving force for the nucleation and growth of crystals.[23,24] The LaMer diagram divides the particle-formation process into three major stages: prenucleation, nucleation, and growth.[22] This diagram proposes that the particle nucleation takes place when the concentration of the active monomer

Received: April 20, 2011
Published: June 27, 2011

reaches a threshold (known as the critical supersaturation point) and ends when the monomer concentration falls below this threshold, resulting in the separation of the nucleation and growth stages during the particle formation,a key to the production of monodispersed nanocrystals. Indeed, Hyeon and co-workers have estimated according to the classical nucleation theory that the nucleation rate can increase 10^{190} with an increase from 2 to 10 in monomer supersaturation.[21]

It is known that the use of the liquid-drop model to assign macroscopic thermodynamic properties (e.g., solubility) to nanometer-sized systems is inaccurate and can cause classical nucleation theory failures in predicting nanocrystal nucleation kinetics.[23−26] In many cases, however, the predictions of the classical nucleation theory cannot be directly verified through experiments because of the inability to measure the concentration of the active monomers in the formation of nanocrystals as well as the inability to identify the chemical nature of these active monomers. A knowledge gap also exists in the understanding of the chemical reactions yielding these active monomers and nuclei. These chemical reactions have long been thought to be complex reactions, which may include multiple reversible, parallel, and/or consecutive elementary steps, because a simple crystal unit cell consists of many atomic components (for example, to construct a CdSe nanocrystal of one unit cell needs at least 18 atoms).[27] The complicated nature of these chemical reactions raises a serious question as to whether it is meaningful to use the concentrations of precursors to estimate those of the active monomers (for example, a reversible reaction could substantially block the direct correlation between the concentrations of precursor and the active monomers).[25,26,28]

To fully understand the nucleation and growth of nanocrystals, it is essential to gain new knowledge on the nature of active monomers and the chemical reactions yielding them. In general, the nanocrystal nucleation process, a crystallization process, should include exothermic reactions because crystals intrinsically possess large lattice energies,[29,30] but these exothermic reactions have yet to be investigated. To explore the existence of such exothermic reactions, we herein report an approach to use gas bubbles to perturb the reactions in the synthesis of iron oxide nanocrystals. Our results show that such exothermic reactions do exist and they strongly affect the nucleation of iron oxide nanocrystals. This finding suggests that gas bubbles can be used to control the nucleation rate of iron oxide nanocrystals.

In the following sections, we first describe and discuss our experimental results that gas bubbles generated from boiling solvents under atmospheric pressure (or under vacuum) can facilitate the formation of iron oxide nanocrystals. Second, we present our results that artificial argon bubbles can replace the solvent gas bubbles in controlling the nucleation and growth of iron oxide nanocrystals. Third, we report our mechanistic studies on the separation of the nucleation and growth in the synthesis of iron oxide nanocrystals using perturbation with Ar gas bubbles. Lastly, we provide some general remarks on the chemical reactions involved in the formation of iron oxide nanocrystals.

RESULTS AND DISCUSSIONS

Iron Oxide Nanocrystal Synthesis System. The synthesis system used in this work is a NIS system that was modified from the synthesis method developed by Hyeon and co-workers.[9] This synthesis system includes only three components: iron oleate as the precursor, oleic acid as the ligand, and long chain hydrocarbon solvents such as 1-octadecene (ODE). After the reaction solution is heated to elevated temperatures (e.g., 300 °C), the thermal decomposition of iron oleate takes place and leads to the formation of iron oxide nanocrystals that consist of magnetite (Fe_3O_4) and maghemite (γ-Fe_2O_3, Supporting Information Figure S1). The composition of these iron oxide nanocrystals can be written in the form of $(Fe_3O_4)_x(Fe_2O_3)_{1-x}$ where x ranges from 0.5 to 0.7 depending on their size.[9] CO_2 and H_2 have been identified as byproducts of the iron oleate decomposition reactions,[21,31−33] but the detailed reactions that lead to the nucleation and growth of iron oxide nanocrystals have not yet been identified.

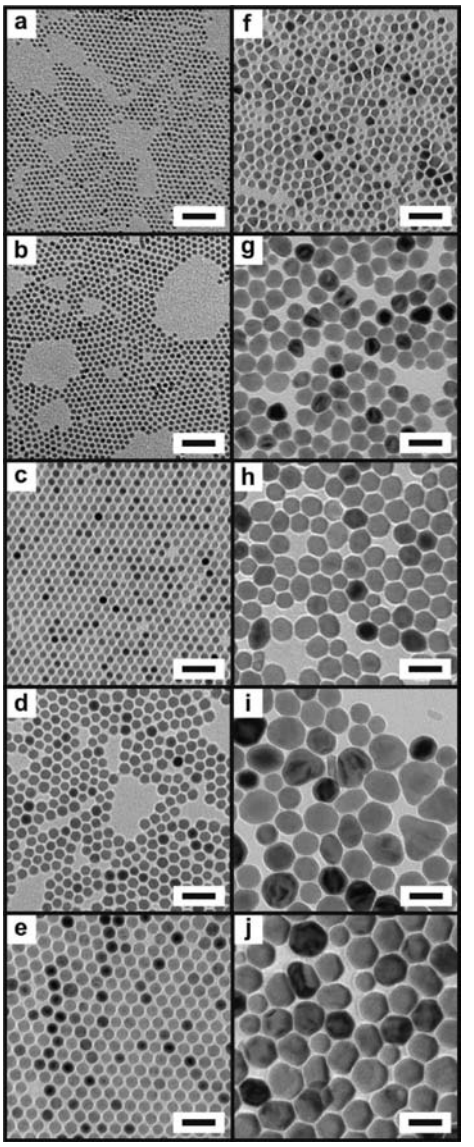

Figure 1. TEM images of iron oxide nanocrystals from the syntheses in boiling solvents (a−e) and nonboiling solvents (f−j) at the reaction temperature of 290 °C (a and f); 300 °C (b and g); 320 °C (c and h); 340 °C (d and i); and 365 °C (e and j). The size of the resulting particles is (a) 5.2 ± 0.4 nm, (b) 6.5 ± 0.3 nm, (c) 9.9 ± 0.4 nm, (d) 13.5 ± 1.0 nm, (e) 16.7 ± 1.1 nm, (f) 12.3 ± 2.1 nm, (g) 27.1 ± 5.6 nm, (h) 33.9 ± 10.4 nm, (i) 41.9 ± 12 nm, and (j) 44 ± 8.5 nm. All scale bars are 50 nm.

A prerequisite for making monodispersed iron oxide nanocrystals by Hyeon's method is the very slow heating of the reaction

system to an elevated target temperature (e.g., 3.3 °C/min).[9,21] A fast heating (e.g., 10 °C/min) of the reaction solution often yields polydispersed and/or irregular shaped iron oxide nanocrystals (Figure S2). Here, we recognize that this prerequisite is strongly associated with the nature and reactivity of the iron oleate precursors that are prepared according to Hyeon's method. We found that the heating rate in the iron oxide synthesis can be increased up to 25 °C/min if the iron oleate precursor was further treated by placing it under a vacuum of 50 mtorr overnight and then aging it in a desiccator at room temperature for two days. The resulting iron oxide nanocrystals exhibit a typical size distribution which is at least comparable to that of those particles made by the slow-heating method with untreated iron oleate precursors (Figure 1a−e).

This result should be due to the fact that the precursor treatment can alter the reactivity of iron oleate precursors: high-vacuum pumping can remove the trace amounts of solvent molecules (e.g., water and ethanol) from iron−oleate complexes, and the subsequent aging allows the iron−oleate complexes to form a uniformed and polymerized structure with a uniform reactivity. Reaction precursors with uniform reactivity have been found to be important in promoting the burst of nucleation in the synthesis of monodispersed group II-VI semiconductor nanocrystals.[8] In addition, aging effects on precursor reactivity were also observed by Peng et al. in the synthesis of CdSe nanorods.[34]

Although they had to use the slow-heating method to produce monodispersed iron oxide nanocrystals, Bronstein et al. also identified the chemical nature of iron oleate as an important factor in iron oxide nanocrystal synthesis.[35] They found that a thermal treatment of the iron oleate precursor can improve the quality of iron oxide nanocrystals. In addition, we herein found that a long period of aging (e.g., two to three months) of iron oleate precursor also affects the synthesis and can yield polydispersed iron oxide nanocrystals. Fortunately, this effect is not observable (or negligible) in relatively short precursor-aging times (e.g., three weeks), which enables us to perform the following mechanistic studies to assess the gas-bubble effects on the nucleation and growth of iron oxide nanocrystals using the same batch of iron oleate precursor.

The Effects of Solvent Gas Bubbles Generated from Boiling Solvents. The synthesis of monodispersed iron oxide nanocrystals in a boiling solvent system has been well documented in the literature.[9,36] To evaluate whether solvent-gas bubbles affect the formation of iron oxide nanocrystals, we carried out two sets of experiments (boiling vs nonboiling) at five different temperatures ranging from 290 to 365 °C. The concentration of iron oleate precursor and oleic acid ligand was kept constant in these syntheses. Four types of long-chain hydrocarbon solvents were used to create the boiling or nonboiling reaction environments at these reaction temperatures: *n*-docosane (DCA), 1-octadecene (ODE), *n*-tetracosane (TCA), and 1-tetradecene (TDE). Pure ODE (or DCA) was used as a boiling solvent at 320 °C (or 365 °C). Two-solvent mixtures, TDE/ODE at a mass ratio of 7:13 or 1:4 and ODE/DCA at 2:3, were used to create boiling environments at 290, 300, and 340 °C, respectively (Table S1). The nonboiling systems were also created using either a pure solvent or a mixture of two solvents.

In a typical experiment, iron oleate (1.0 mmol), oleic acid (0.55 mmol), and a pure or mixed long-chain hydrocarbon solvent (5 g) were added in a three-neck flask, and the mixture was heated to an elevated reaction temperature under stirring at a heating rate of ∼18 °C/min. This reaction temperature was maintained for 60 min, and the synthesis was terminated by cooling the reaction solution to room temperature. This synthesis was carried out under argon atmosphere using a Schlenk line. The resulting iron oxide nanocrystals were purified by a triple precipitation/redispersion treatment using acetone and hexane.

Transmission electron microscope (TEM) observations show that the syntheses in boiling and nonboiling solvents resulted in iron oxide nanocrystals with striking differences in their size, shape, and size distributions (Figure 1). The syntheses in boiling solvents yielded spherical particles with sizes of 5.2, 6.5, 9.9, 13.5, and 16.7 nm at a respective reaction temperature of 290, 300, 320, 340, and 365 °C (Figure 1a−e). These nanocrystals have typical size distributions less than 6%. In contrast, the syntheses in nonboiling solvents yielded irregular shaped polyhedrons that exhibit a much larger average size (∼3 times) than those spherical nanocrystals made in the boiling synthesis at identical corresponding reaction temperatures (Figure 1f−j). The formation of large-sized particles indicates that fewer nuclei formed in the nonboiling synthesis than in the boiling reactions.[23,24] For a given amount of precursor, a greater number of nuclei yields a smaller final size of nanocrystals, and vice versa. We speculate that the solvent gas-bubbles generated from the boiling solvents facilitate nucleation in these boiling syntheses. The next question is whether these solvent-gas bubbles also affect the crystallization yield (or reaction yield) of iron oxide nanocrystals in these syntheses. The iron oxide crystallization yield is the overall result of both the nucleation and growth of iron oxide nanocrystals in a synthesis.

Iron Oxide Reaction Yield. To determine the bubbling effects on iron oxide crystallization yields, we conducted three parallel syntheses in boiling or nonboiling conditions at 300 °C using an ODE/TDE mixture as the boiling solvent and pure ODE as the nonboiling reaction solvent. These syntheses were carried out using an identical concentration of iron oleate and oleic acid with a heating rate of 18 °C/min. After 1 h at 300 °C, we thoroughly purified the resulting iron oxide nanocrystals. Special care was taken to minimize the loss of product during purification. The iron oxide nanocrystals were dried at 50 °C in a vacuum oven, and the mass percent of ligand molecules on these particles was measured by thermogravimetric analysis (TGA, Figure S3). Then, the experimental iron oxide crystallization yield was calculated via dividing the actual weight of the ligand-free iron oxides by the theoretical reaction yield. An average yield of 77 ± 4% was found for the iron oxide synthesis under the boiling condition, whereas a yield of 57 ± 1% was determined for the synthesis under the nonboiling condition (Table S2). The average crystallization yields were calculated from the results of three typical reactions. Although there may exist a systematic error in this TGA-based method, the relative standard deviations of these experimental results are small (less than 5%), and thus, the difference between them is obvious. We further performed a "Student's *t* test" to analyze the difference between these two reaction yields, and the analysis shows that the $t_{calculated}$ is greater than t_{table} at the 99.5% confidence level (or *p*-value of 0.005).[28] This result strongly suggests the difference between the two experimental results is indeed significant, demonstrating that solvent-gas bubbles indeed increase the overall iron oxide crystallization yield in the synthesis under the boiling condition when compared to the synthesis under the nonboiling condition.

An argument might arise that the relatively lower crystallization yield observed herein for the nonboiling syntheses could

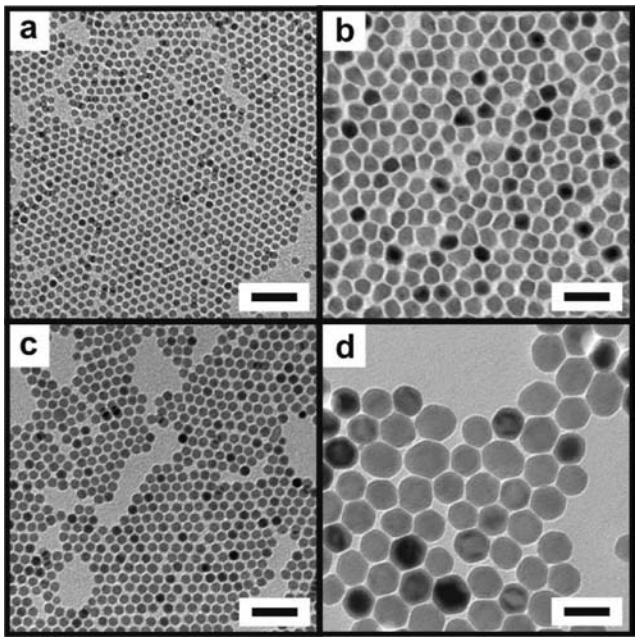

Figure 2. TEM images of iron oxide nanocrystals synthesized in boiling solvents under reduced pressures (a and c) and in nonboiling solvents under 1 atm (b and d). The syntheses with pure ODE as the solvent and reaction temperature at 300 °C (a and b): the resulting particles exhibit (a) 7.3 ± 0.3 nm and (b) 18.3 ± 3.4 nm in diameter. The syntheses with pure TCA as the solvent and reaction temperature at 320 °C (c and d): the resulting particles exhibit (c) 9.4 ± 0.4 nm and (d) 36.8 ± 5.6 nm in diameter. All scale bars are 50 nm.

be due to greater product loss during sample purification. However, the iron oxide nanocrystals made from the nonboiling syntheses exhibit a significantly larger size than those from the boiling syntheses (Figure 1). These larger sized particles are relatively easier to precipitate out from reaction solutions than the smaller ones. In this sense, we should have less product loss in the case of nonboiling reactions than in the boiling syntheses. Altogether, these results further suggest that the solvent-gas bubbles can impact both the nucleation and growth of iron oxide nanocrystals via affecting iron oxide crystallization yield. Another argument is that the observed gas-bubble effects could originate from the slight differences in solvent compositions used in these synthesis. To investigate this possibility, we performed iron oxide synthesis under boiling conditions created by reduced pressures.

The Effects of Solvent-Gas Bubbles Generated from Boiling Solvents with Reduced Pressure. We performed two sets of iron oxide nanocrystal syntheses (boiling vs nonboiling) with identical solvents, reaction temperatures, and the concentrations of iron oleate and oleic acid. ODE and TCA were used as solvents to perform the iron oxide syntheses at 300 and 320 °C, respectively. The boiling syntheses were achieved by precisely controlling the reduced pressure of the reaction systems with a vacuum pump (Figure S4). The typical temperature fluctuations in our experiment were within ±3 °C, which is similar to the temperature fluctuations observed in the corresponding nonboiling syntheses. TEM observations show that significant differences exist between these boiling and nonboiling syntheses: the boiling reactions yielded smaller spherical nanocrystals with a narrow size distribution, while the nonboiling counterpart reaction resulted in larger iron oxide polyhedrons with a poor size distribution (Figure 2b,d). The size and size distribution of the iron oxide nanocrystals made by the boiling syntheses under reduced pressures are similar to those particles made by the synthesis under naturally boiling conditions at the same temperatures (Figures 2a,c, and 1b,c). These results rule out the possibility that the solvent composition plays a major role in controlling the nucleation and growth of iron oxide nanocrystals.

In general, boiling solvents can give rise to three major effects on nanocrystal formation: (1) providing low free-energy solvent-gas interfaces, (2) promoting mass transfer, and (3) increasing the heat transfer coefficient of the reaction solutions.[2,37] It has been found that the low free-energy interfaces created by solvent-gas bubbles are preferential sites for the heterogeneous nucleation of additional gas bubbles.[23,24,38] The free energy of bubble gas/liquid interfaces is determined by the surface tension of the liquid. The surface tension of long-chain hydrocarbon solvents (e.g., ODE) is more than 50 times smaller than that of solid iron oxides,[39,40] and therefore, the gas/liquid interfaces of these bubbles unlikely serve as the preferential sites for promoting the heterogeneous nucleation of iron oxide nanocrystals.

The second effect of solvent-gas bubbles is on mass transfer and takes place by increasing the convection rate of the reaction solutions owing to the formation and growth of the bubbles, but this increase in mass transfer is substantially smaller than that of the forced convection created by the vigorous magnetic stirring (~1100 rpm) in our experiments. In other words, the effect on mass transfer unlikely plays a major role in affecting the formation of iron oxide nanocrystals observed herein. Therefore, boiling bubble-enhanced heat transfer should be the major cause for the observed effects on the nucleation and growth of iron oxide nanocrystals.

It is known that boiling can significantly increase the heat transfer coefficient of a solvent because of the latent heat transfer, a process of giving off or absorbing heat without changing temperature.[2,37,41,42] Boiling-induced latent heat transfer, giving off and absorbing heat simultaneously, has been used in many technological applications related to energy production such as the cooling of nuclear reactors.[42] In the case of iron oxide nanocrystal synthesis, boiling heat transfer can promote both the endothermic and exothermic chemical reactions that occur during nanocrystal formation. The thermal decomposition reactions of iron oleate are endothermic, whereas the formation of iron oxide crystal lattices includes exothermic reactions. A fundamental question is whether the endothermic decomposition reactions or exothermic crystallization reactions dictate the formation of iron oxide nanocrystals. To address this question, we designed experiments using artificial bubbles generated by a room-temperature Ar flow (Figure S5). Although the "cold" Ar bubbles can absorb only limited amounts of heat from the surrounding hot reaction solution due to their small molar heat capacity,[43] the presence of these bubbles can substantially facilitate the evaporation of the surrounding hot solvent molecules,[2,37] which can absorb a larger amount of heat from the reaction solution. Together, these processes, which only absorb latent heat from the reaction solution, provide a unique local microenvironment for specifically promoting the exothermic reactions during the formation of iron oxide nanocrystals.

The Effects of Ar Bubbles. To explore the Ar-bubble effects, we conducted three types of iron oxide nanocrystal syntheses with identical concentrations of iron oleate and oleic acid. Both ODE and TCA were used as the solvent for the synthesis at 300 °C, and TCA was used as the solvent for the synthesis at

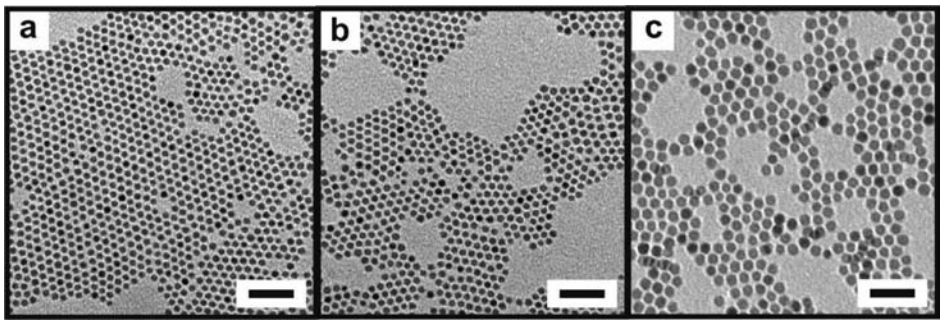

Figure 3. TEM images of iron oxide nanocrystals made from Ar bubbling experiments: particles made in pure ODE as solvent at 300 °C (a) with 6.7 ± 0.4 nm diameter; in pure TCA as solvent at 300 °C (b) with 7.0 ± 0.3 nm in diameter; in pure TCA as solvent at 330 °C (c) with 11.6 ± 0.7 nm in diameter. All scale bars are 50 nm.

330 °C. In these syntheses, the reaction solutions were first heated to an elevated temperature that is 10 °C higher than the target reaction temperature. Once this temperature was reached, we turned on Ar bubbles and adjusted the temperature of the solution to the target temperature (Figure S5). The typical temperature fluctuations in these syntheses were within ±6 °C. After 1 h under Ar bubble flow at the target reaction temperature, the syntheses were terminated and the resulting iron oxide nanocrystals were purified for TEM analysis.

Significantly, these Ar-bubbling syntheses yielded monodispersed, spherical iron oxide nanocrystals like in the case when using boiling bubbles (Figures 3 and 1a−e). The two syntheses at 300 °C resulted in iron oxide nanocrystals with similar sizes in diameter: 6.7 ± 0.4 nm in ODE and 7.0 ± 0.3 in TCA (Figure 3a,b). The sizes of these nanocrystals are also close to the sizes of those particles made via boiling bubbles generated at 1 atm or under a reduced pressure (Figures 1b and 2a). The Ar-bubbling synthesis at 330 °C produced iron oxide nanocrystals of 11.6 ± 0.7 nm in diameter (Figure 3c), and this size lies between the sizes of those particle made by boiling bubbles at 320 and 340 °C (Figure 1c,d). Altogether, these results clearly demonstrate that Ar bubbles can effectively mimic the function of boiling bubbles in controlling the formation of iron oxide nanocrystals.

Importantly, these results also suggest that the exothermic reactions (but not the endothermic reactions) play a dominant role in controlling the formation of iron oxide nanocrystals, since Ar bubbles only promote exothermic reactions. In addition, this Ar-bubble effect enables one to use just one type of solvent to synthesize monodispersed iron oxide nanocrystals over a large size range through tuning of reaction temperature. Furthermore, the Ar-bubble effect provides a novel tool for investigating nanocrystal nucleation and growth. For example, one can probe the mechanism of the nucleation and growth of iron oxide nanocrystals by turning on/off the Ar bubbles under conditions with identical reaction temperatures, solvent types, and concentration of precursors and ligands.

Kinetic Studies on Gas-Bubble Effects. To further assess the effects of gas bubbles on the nucleation and growth of iron oxide nanocrystals, we performed kinetic studies on two sets of syntheses at 300 °C (boiling vs nonboiling, and bubbling vs nonbubbling). Both sets of syntheses used identical concentrations of iron oleate (1 mmol) and oleic acid (0.55 mmol). ODE/TDE (4 g/1 g) was used as the boiling solvent, and ODE (5 g) was used as the solvent in the rest of syntheses. In these experiments, the reaction solutions were heated to the reaction temperature at a rate of 18 °C/min. The moment when the reaction solution was stabilized at 300 °C was set as reaction time zero, and then serial aliquots were taken for kinetic studies using TEM analysis.

In the boiling synthesis, no nucleation was observed until ∼13 min at 300 °C, and 5.1-nm iron oxide nanocrystals were observed at 15 min (Figure 4). As the nanocrystals grew, both their size distribution and growth rate gradually decreased. Iron oxide nanocrystals with diameter of 6.5 ± 0.3 nm were obtained after 1-h reaction (Figure 4d). Afterward, no substantial increase in nanocrystal size was observed, indicating that the nanocrystal growth was complete and the reaction precursors were almost consumed during the 1-h reaction. These results show that, although iron oleate can undergo decomposition at 300 °C,[9,21] reaching this temperature cannot immediately trigger the nucleation of iron oxide nanocrystals in the reaction solution. A similar "delayed-nucleation" phenomenon was previously observed by Alivisatos et al. in the preparation of iron oxide nanocrystals using an injection-based synthesis.[19]

This "delayed-nucleation" phenomenon suggests that nucleation does not strongly depend on the concentration of iron oleate precursors but instead depends on the concentration of iron oleate thermal decomposition products (e.g., "active monomers"). Therefore, this nucleation process should follow the LaMer diagram. With the decomposition of iron oleate precursors and subsequent combination reactions, the active monomer concentration builds up to a threshold that enables nucleation.[22] In addition, these results show that iron oxide nanocrystals display an extremely rapid growth rate at the stage immediately after nucleation: the size of iron oxide nanocrystals can reach 5.1 nm at ∼2 min after nucleation starts (Figure 4a). In addition, our results show that no clear secondary nucleation was observed, which indicates that the separation of nanocrystal nucleation qand growth was well maintained during the boiling synthesis (Figure 4b−d).

In contrast, the nonboiling synthesis displayed completely different nanocrystal formation kinetics (Figure 4e−h). First, the nucleation of iron oxide nanocrystals took place at a later time than that in the boiling synthesis. No nanocrystals were observed until ∼18 min at 300 °C, and both the size- and shape-distribution of the newly formed particles were poor (Figure 4e). These results indicate that solvent bubbles facilitate at least one of the following processes: (1) the formation of active monomers, and/or (2) the creation of nuclei from active monomers.[22] In other words, at least one of these two processes is determined by an exothermic reaction. Second, the iron oxide nanocrystals in the nonboiling synthesis showed a faster growth rate than those

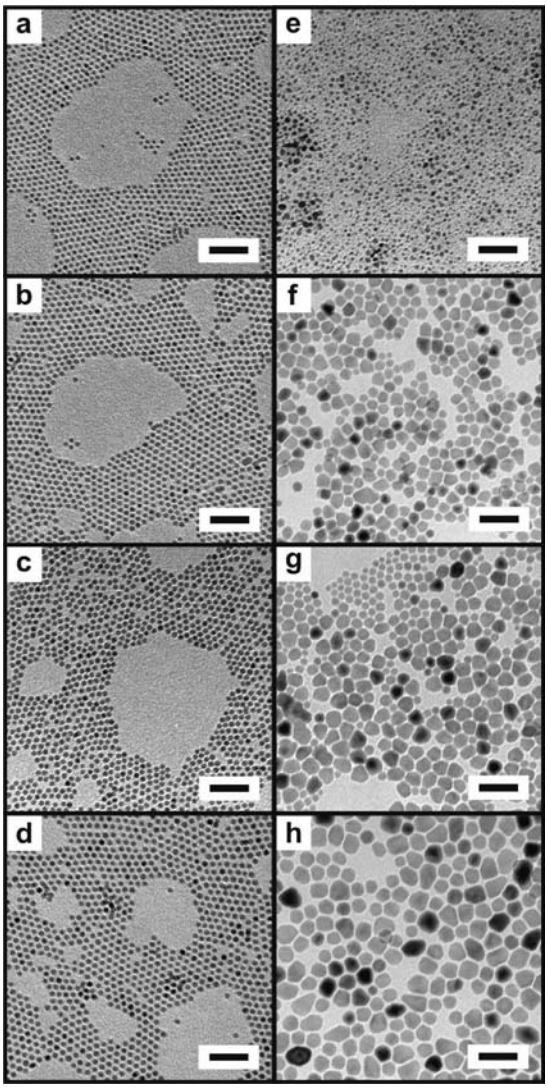

Figure 4. Kinetic study of the syntheses of iron oxide nanocrystals in boiling (a−d) and nonboiling solvents (e−h). TEM images of iron oxide nanocrystals were taken at different reaction times during the synthesis. The moment when the temperature of reaction solution reached 300 °C was counted as the zero reaction time. The resulting particles were taken from the synthesis in boiling solvent at: (a) 15 min (5.1 ± 0.4 nm in diameter), (b) 20 min (5.6 ± 0.4 nm in diameter), (c) 30 min (6.0 ± 0.4 nm in diameter), and (d) 60 min (6.5 ± 0.3 nm in diameter). The resulting particles were taken from the synthesis in the nonboiling solvent at: (e) 18 min (5.1 ± 0.5 nm in diameter), (f) 25 min (15.7 ± 5.8 nm in diameter), (g) 30 min (17.2 ± 6.5 nm in diameter), and (h) 60 min (19.9 ± 4.9 nm in diameter). All scale bars are 50 nm.

in the boiling synthesis, and their shapes appeared as irregular polyhedrons (Figure 4f−h). In addition, a noticeable appearance and disappearance of small sized particles was observed during further particle growth, showing that secondary nucleation and Ostwald ripening occurred in the synthesis (Figure 4f−h). These results, together with the results showing that nonboiling syntheses had a low iron oxide crystallization yield, further confirm that the nonboiling synthesis yielded fewer nuclei when compared with the boiling synthesis. In addition, these results further suggest that the nucleation and growth of iron oxide nanocrystals follow the LaMer diagram.[22] When compared with the synthesis using boiling solvents, this nonboiling synthesis produced fewer iron oxide nuclei, and thus, the subsequent growth of these nuclei cannot consume an adequate amount of active monomers and/or the chemical species that can produce these active monomers in order to decrease the concentration of active monomers below the nucleation threshold. As a consequence, secondary nucleation took place as observed in the nonboiling synthesis (Figure 4e−h).

To further explore the mechanism of the formation of iron oxide nanocrystals, we carried out kinetic studies on two types of syntheses at 300 °C with controlled Ar-bubble flow. In the first synthesis, the Ar bubbles flowed continuously during the entire reaction period, and this synthesis displayed nearly identical kinetics to the boiling synthesis (Figures 5a−d and 4a−d). After 15 min, iron oxide nanocrystals of 4.3 nm in diameter with a size distribution of 9.3% had appeared. During further growth, the size distribution and growth rate of the iron oxide nanocrystals decreased monotonically, and 6.7-nm nanocrystals were obtained after 1-h reaction (Figure 5a−d). These results confirm that Ar bubbles can replace boiling bubbles in controlling the colloidal synthesis of monodispersed iron oxide nanocrystals, suggesting that an exothermic reaction should be the rate-limiting step in the formation of iron oxide nanocrystals.

In the second synthesis, we turned off the Ar-bubble flow after 15 min, and the iron oxide nanocrystals formed at this moment exhibited nearly identical size and size distribution to those made in the first Ar-bubbling synthesis at the same reaction time (Figure 5e−h). However, after only 5 min in the absence of Ar-bubbles, a distinguishable change in the kinetics of nanocrystal formation was observed: the mean size of the resulting nanocrystals (4.7 nm) was slightly smaller than that of those particles (5.6 nm) formed in the synthesis with continuous Ar-bubble flow, while their size distribution widened due to the presence of small-sized particles (3−4 nm). Owing to the presence of a large quantity of unreacted precursors during this early reaction time (15−20 min), these small-sized particles should be created via secondary nucleation but not via the dissolution of large particles through an Ostwald ripening process. As further reaction took place, the iron oxide nanocrystals with the average size gradually grew, while small particles (3−4 nm) continuously formed and then grew. After 1-h reaction, the resulting nanocrystals exhibit a broad Gaussian-shaped size distribution centered at ∼6.8 nm and a continuous tail to 3 nm in diameter (Figure 5h).

These results clearly show that continuous secondary nucleation events took place after Ar bubble flow was turned off, which indicates that the primary nucleation of iron oxide nanocrystals was incomplete under 15-min Ar bubbling. In other words, this primary nucleation did not produce a sufficient amount of iron oxide nuclei whose subsequent growth could bring the active-monomer concentration below the nucleation point, and thus, nearly continuous secondary nucleation was observed after the Ar bubbles were turned off (Figure 5f−h). Multiple nucleation events were also observed in the nonboiling synthesis at 253 °C (Figure S6).

To further explore the kinetics in the nucleation of iron oxide nanocrystals, we carried out two additional iron oxide syntheses in which the Ar bubble flow was turned off at 12 or 18 min (Figure 6). The syntheses were conducted at 300 °C for 1 h and the resulting particles were purified for TEM analysis. Amazingly, the synthesis with 18-min Ar bubbling yielded monodispersed iron oxide nanocrystals of 7.0 nm (Figure 6b), which is just

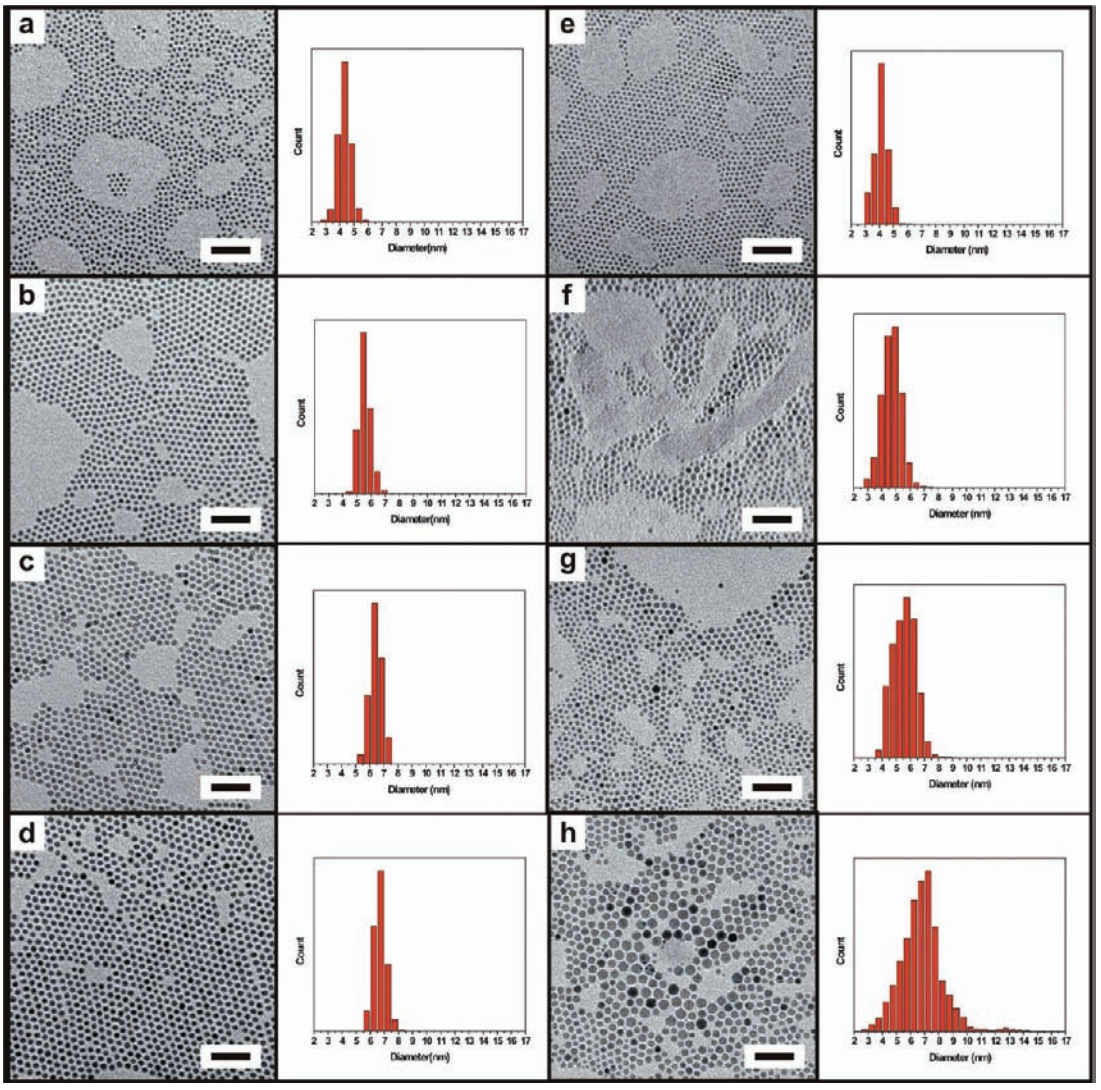

Figure 5. Kinetic study of the synthesis of iron oxide nanocrystals under controlled Ar bubbling. TEM images of iron oxide nanocrystals taken from the synthesis in pure ODE at 300 °C under Ar bubbling through the entire synthesis at (a) 15 min (4.3 ± 0.4 nm in diameter), (b) 20 min (5.6 ± 0.4 nm in diameter), (c) 30 min (6.4 ± 0.4 nm in diameter), and (d) 60 min (6.7 ± 0.4 nm in diameter). TEM images of iron oxide nanocrystals taken from the synthesis in pure ODE at 300 °C with 15-min Ar bubbling at (e) 15 min (4.2 ± 0.3 nm in diameter), (f) 20 min (4.7 ± 0.7 nm in diameter), (g) 30 min (5.6 ± 0.8 nm in diameter), and (h) 60 min (6.8 ± 1.5 nm in diameter). The corresponding particle size distribution histograms are shown in the right side in these panels. All scale bars are 50 nm.

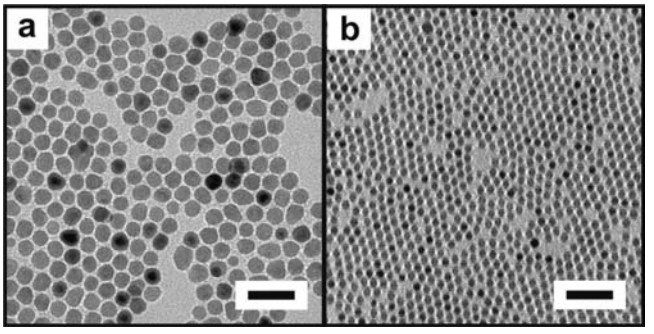

Figure 6. TEM images of iron oxide nanocrystals run in pure ODE at 300 °C for 60 min with (a) 12-min Ar bubbling, 17.9 ± 2.9 nm diameter, and (b) 18-min Ar bubbling, 7.0 ± 0.5 nm diameter. Scale bars are 50 nm.

slightly larger than those particles made in the synthesis under continuous Ar bubbling (Figure 5d). This result suggests that the reaction under 18-min Ar bubbling produced an adequate amount of nuclei whose growth could prevent secondary nucleation events. The result further indicates that Ar bubbles displayed a larger effect on the nucleation of iron oxide nanocrystals than their growth, because the growth of iron oxide nanocrystals was not substantially affected in the absence of Ar bubbles (Figure 6b). Importantly, this result reveals that the nature (or properties) of chemical reactions associated with the nucleation is different from those reactions related to nanocrystal growth. This difference could be a chemical origin for achieving the separation of nucleation and growth during solution-phase synthesis (vide infra).

On the contrary, the synthesis with 12-min Ar bubbling yielded irregular shaped iron oxide nanocrystals that are similar to those made in the nonboiling synthesis (Figures 6a and 1g), suggesting that these two syntheses had similar nanocrystal-formation kinetics. Taken together, these results further demonstrate that Ar bubbles played a very important role in promoting

Scheme 1. Reaction Scheme Illustrating (a) the Formation of Thermal Free Radicals during the Endothermic Decomposition of Iron Oleate and the Exothermic Formation of Primary Iron Oxide Clusters, (b) the Formation of 1-D Iron Oxide Clusters via Exothermic, Single-Bond Forming Reactions, and (c) the Creation of 2-D Iron Oxide Clusters via Highly Exothermic, Multiple-Bond Forming Reactions

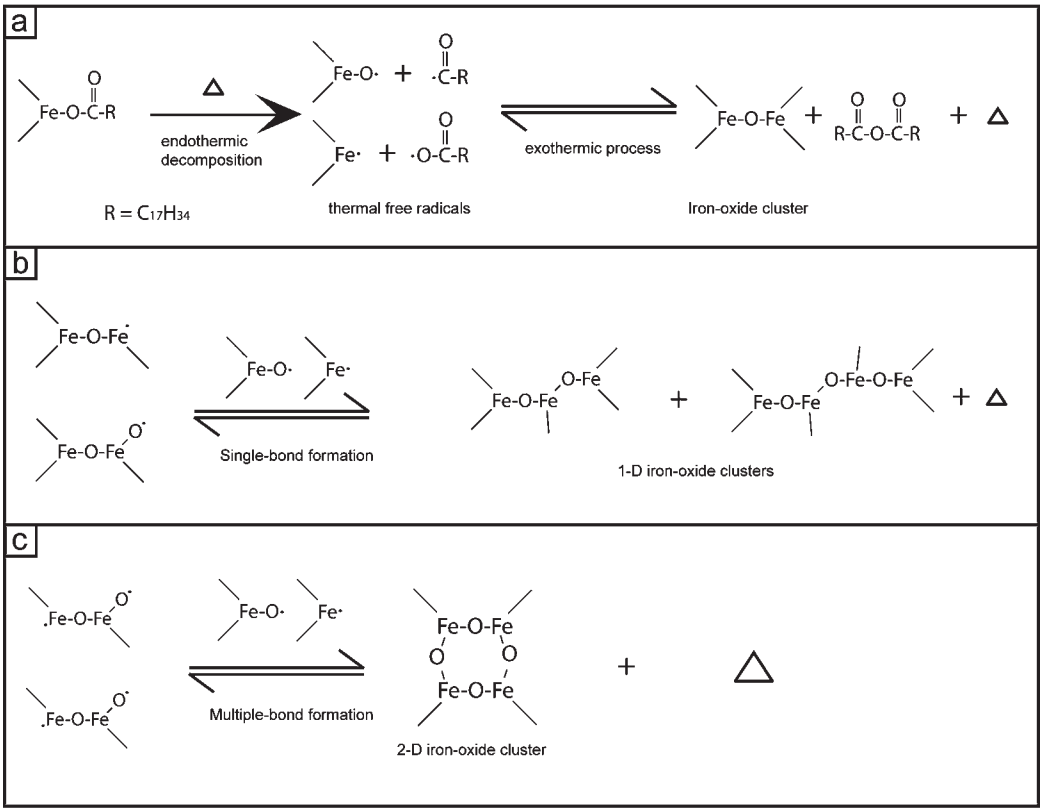

the nucleation of iron oxide nanocrystals. In addition, these results further suggest that the separation of the nucleation and growth of iron oxide nanocrystals are under a fragile kinetic balance (unlike a permanent separation suggested by the original LaMer diagram).[22] This balance can be easily broken if the subsequent growth of nanocrystals cannot keep the active-monomer concentration below the nucleation threshold. Therefore, there exists a prerequisite for an effective separation of these two stages: the primary nucleation should produce a critical (or sufficient) amount of nuclei whose subsequent growth can prevent secondary nucleation events.

GENERAL DISCUSSIONS

The formation of nanocrystals is a crystallization process at the nanometer scale. In general, a crystal unit cell forms the smallest crystal possible, and thus, the nuclei of nanocrystals should have a size similar to that of their crystal unit cell. For example, a magnetite (Fe_3O_4) nanocrystal of a single unit cell contains 62 oxygen atoms and 39 iron atoms with more than 100 bonds between these atoms.[44] The nucleation of iron oxide nanocrystals should include a complex reaction with multiple steps of successive addition of simple monomers that are generated by the thermal decomposition of iron oleate precursors. These addition reactions together with other types of reactions such as elimination, substitution, and rearrangement reactions can yield various types of interconvertible iron oxide clusters, and these clusters can exhibit 1-, 2-, or 3-D (dimensional) structures.

Here, we refer to the "active monomers" in this synthesis as the clusters involved in the reactions that directly yield nuclei. When the concentration of active monomers reaches a threshold, nucleation takes place. Although the detailed molecular mechanisms of these reactions are not clear yet, our results show that the nucleation of iron oxide nanocrystals is strongly related to an exothermic reaction because this process can be promoted by gas bubbles through latent heat absorption.[2,37,41] In addition, our results show that the gas bubbles have more influence on the nucleation of nanocrystals than on their growth (Figures 5d and 6b), which indicates that the nucleation and growth of iron oxide nanocrystals may depend on different types of iron oxide clusters which undergo chemical reactions with different heat releasing capacities.

The thermal decomposition of iron−oleate complexes is the primary step in the synthesis of iron oxide nanocrystals, and this process includes endothermic reactions that may take place through the formation of thermal free radicals (Scheme 1). Subsequently, the resultant free radicals can undergo addition and/or substitution reactions with iron−oleate complexes, yielding larger iron oxide clusters, which can further decompose to form free radicals. The combination of these iron oleate containing free radicals includes exothermic processes, and the inter- and intramolecular combination of the free radicals can result in iron oxide clusters with 1-D, 2-D, or 3-D structures.[45]

The nucleation of nanocrystals is a phase transition process that creates crystalline nuclei from "amorphous" active monomers.[23,24]

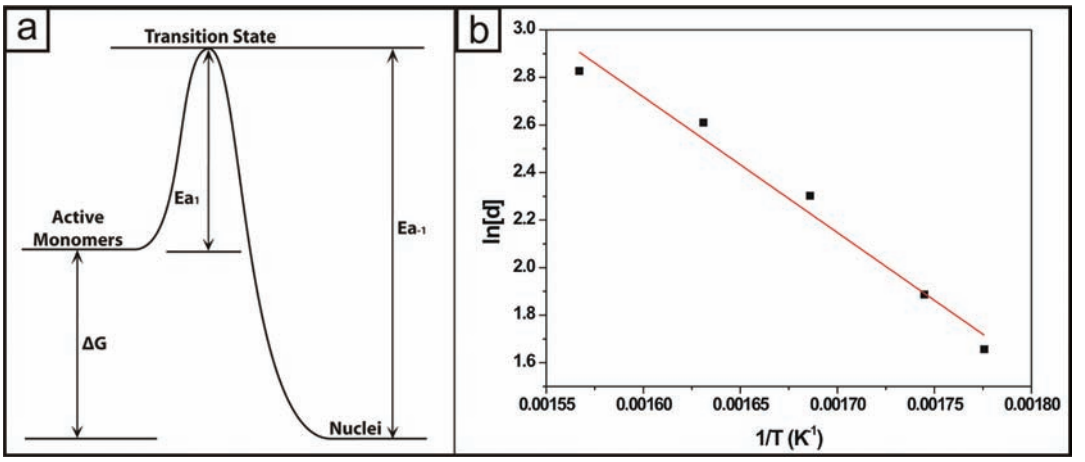

Figure 7. (a) Reaction coordinate diagram describing the formation of iron oxide nanocrystal nuclei from active monomers, and (b) a plot of the natural logarithm of nanocrystal diameter as a function of inverse reaction temperature in Kelvin.

Thus, the chemical reactions that are directly associated with the nucleation should largely depend on multiple-bond forming processes that can release an extremely large amount of heat locally. For example, the formation of three Fe−O bonds can release 1221 kJ/mol.[46] The release of such an extremely large amount of local heat can in turn promote the occurrence of the reverse reaction, the thermal decomposition of the transition species in the formation of nuclei, and decrease the yield of the forward nucleation reaction. Solvent boiling (or Ar) bubbles can absorb the local heat through latent heat transfer, and hence lead to a substantial increase of the nucleation yield in the formation of iron oxide nanocrystals as observed in this work.

In contrast to nucleation, the growth of iron oxide nanocrystals is not a phase transition process and thus can be achieved by chemical reactions that take place on the surface of these nanocrystals. A single-bond formation reaction can lead to the growth of nanocrystals, and therefore, multiple-bond forming reactions are not essential for nanocrystal growth. A single-bond formation reaction releases less local heat than multiple-bond formation reactions, and this reaction can take place with iron oxide clusters other than active monomers. Because their formation free energies are lower than that of the active monomers, these iron oxide clusters should have a greater abundance than those of the active monomers in the reaction solution during an iron oxide nanocrystal synthesis. Therefore, the growth of iron oxide nanocrystals can be dominated by these low-heat-releasing, single-bond formation reactions. In other words, nanocrystal growth should not be strongly affected by the gas-bubble induced latent heat transfer, which is consistent with our results (Figure 6b).

Moreover, the identification of exothermic reactions is further consistent with the results from the iron oxide nanocrystal syntheses in boiling solvents at temperatures ranging from 290 to 365 °C. These syntheses yielded iron oxide nanocrystals with final sizes dependent on reaction temperature: a higher temperature yielded larger particles, and vice versa (Figure 1). Therefore, the synthesis with a higher reaction temperature yielded fewer nuclei because the amount of iron oleate precursor is equal among these syntheses. This result clearly shows that a higher reaction temperature hinders the nucleation of iron oxide nanocrystals. This temperature effect further indicates that the rate-determining step in the nucleation of iron oxide nanocrystals is a reversible (or a quasi-reversible) reaction in which the forward nucleation reaction is an exothermic process.[28,29] According to Le Chatelier's principle, decreasing reaction temperature can cause such a reversible reaction go toward the exothermic process.[28,29]

These experimental results can provide a semiquantitative analysis on the enthalpy of this reversible reaction if we assume that (1) the equilibrium of this reversible reaction is achieved at the end of the primary nucleation stage,[47−49] (2) the concentration of the active monomers (the reactant) is at a nucleation threshold that is independent of reaction temperatures in the range of 290−365 °C, and (3) the crystallization yield is consistent in these boiling syntheses. Therefore, the concentration of nuclei can be presented by eq 1.

$$[\mathrm{N}] = K[AM]^a \tag{1}$$

where [N] denotes the nucleus concentration, [AM] is the concentration of active monomers, a represents the reaction order, and K is the equilibrium constant of the reaction. If the forward and backward reactions obey Arrhenius kinetics, K can be written as a function of the reaction temperature, the difference between the activation energies of the forward and backward reactions ($\Delta G = E_{a1} - E_{a-1}$), and the ratio of their pre-exponential factor ($A = A_1/A_{-1}$).

$$K = \frac{A_1 e^{-E_{a1}/RT}}{A_{-1} e^{-E_{a-1}/RT}} = A e^{-\Delta G/RT} \quad \text{or} \quad \ln K = \ln A - \Delta G/RT \tag{2}$$

On the basis of the assumption of a consistent crystallization yield in these syntheses, we can describe the nucleus concentration as follows,

$$[\mathrm{N}] = \frac{\Phi[\mathrm{P}]}{\left\{\frac{4}{3}\pi\left(\frac{d}{2}\right)^3 D\frac{F}{MW}\right\}} \tag{3}$$

where [P] stands for the initial precursor concentration, Φ is crystallization yield, d is the average diameter of the nanocrystal product calculated from their mean volume, D is the density of iron oxide, MW is the molar molecular weight of iron oxide, and

F is the number of iron atoms in the molecular formula of iron oxide. We assume that the resulting nanocrystal products exhibit a constant composition of magnetite and maghemite in the syntheses at these reaction temperatures, and thus, D and MW are constant in the equation. The combination of eqs 1−3 gives eq 4,

$$\ln d = \frac{\Delta G}{3RT} - \frac{a}{3}\ln[AM] + \frac{1}{3}\ln C \quad (4)$$

where $C = (6\Phi[\mathrm{P}]\mathrm{MW}/\pi FDA)$ and is constant in our experiments.

During the primary nucleation stage, the concentration of active monomers is above the nucleation threshold. If the variation of active-monomer concentration is very small during this nucleation stage, eq 4 states that the natural logarithm of nanocrystal diameter (d) is inversely proportional to reaction temperature if ΔG is constant. Indeed, using our experimental results in a plot of ln d as a function of $1/T$ yielded a good linear relationship with a percentage of variance of 0.97 in least-squares fitting (Figure 7). The slope of this fitting line gives the reaction enthalpy of the nucleation formation as -142 ± 12 kJ/mol. This large negative heat of reaction is consistent with our observation that gas bubbles can significantly promote the nucleation of iron oxide nanocrystals. This result further demonstrates that the nucleation of iron oxide nanocrystals is determined by the chemical reaction kinetics.

This temperature dependent nucleation effect contradicts the prediction of classical nucleation theory, which suggests that the number of nuclei can increase with an increase in nucleation temperature.[22,38] This contradiction should be due in large part to the fact that classical nucleation theory does not include the kinetics of chemical reactions between precursors. Moreover, the temperature effect is also different from the recent observation by Peng et al. in the synthesis of InP nanocrystals, where they found the number of nuclei increased with an increase in reaction temperature with a fairly small activation energy of ~11 kJ/mol.[25] This difference may arise from the difference in the two nanocrystal synthesis systems.

Furthermore, our results provide new insights into the separation of the nucleation and growth of nanocrystals. Nanocrystal growth competes with nucleation, and the growth of iron oxide nanocrystals consumes the active monomers as well as the iron oxide clusters that can form these active monomers. As a consequence, the concentration of active monomer is reduced below the nucleation threshold, terminating the nucleation. Our results show that the separation of nucleation and growth of iron oxide nanocrystals is under a fragile balance, which can be easily broken during the subsequent nanocrystal growth, leading to secondary nucleation (Figure 5h).

In addition, our results show that a critical number of nuclei must be formed during the primary nucleation in order to effectively prohibit secondary nucleation in a closed synthesis system (Figure 6b). Even if the primary nucleus number is smaller than this critical number, primary nucleation can also be stopped by the growth of newly formed nanocrystals. However, as the growth rate of iron oxide nanocrystals decreases with an increase in their size, the growth of iron oxide nanocrystals cannot consume a sufficient amount of active monomers or the clusters that can form these active monomers. As a result, the concentration of active monomers can reach the nucleation threshold resulting in secondary nucleation, which was observed in the synthesis with nonboiling solvents (Figures 4e−h and 5f−h). These results suggest that the control of the primary nucleation rate is critical in the synthesis of monodispersed colloidal nanocrystals.

It is worth noting that gas-bubbling effects can be observed in a synthesis of nanocrystals of other compositions if this synthesis can meet the following conditions: (1) there exist both endothermic and exothermic reactions in the synthesis, and (2) one of the exothermic reactions is the rate-limiting step in the complex reactions associated with nanocrystal's nucleation and/or growth, or a process competing with nanocrystal's nucleation or growth. We hope that gas bubbles can be used as an effective tool to probe the mechanisms of the nucleation and growth of other nanocrystal systems.

CONCLUSIONS

We performed a mechanistic study of colloidal iron oxide nanocrystal synthesis by comparing boiling versus nonboiling solvents as well as the effects of Ar-bubbling. We observed that solvent boiling bubbles or Ar bubbles can substantially promote the primary nucleation of iron oxide nanocrystals, which can successfully suppress secondary nucleation and yield monodispersed nanocrystal products. We identified that bubbling effects take place through absorbing local latent heat released from the exothermic reactions involved in the nucleation and growth of iron oxide nanocrystals. Our results suggest that the nucleation and growth of iron oxide nanocrystals depend on different types of chemical reactions. The growth of iron oxide nanocrystals may primarily depend upon single-bond formation reactions, whereas the nucleation strongly relies on the multiple-bond formation reactions than can release much larger amounts of reaction heat than those single-bond formation reactions.

The identification of exothermic reactions is further consistent with our results from the synthesis of iron oxide nanocrystals with boiling solvents at temperatures ranging from 290 to 365 °C. On the basis of these experimental data, we determined the reaction enthalpy in the nucleation of iron oxide nanocrystals to be -142 ± 12 kJ/mol. Furthermore, our results show that the separation of the nucleation and growth of iron oxide nanocrystals is under a delicate balance which can be easily broken during the subsequent growth of nanocrystals. These results suggest that a prerequisite for effectively suppressing secondary nucleation is that the primary nucleation must produce a critical amount of nuclei, and this finding is important for *a priori* design of colloidal synthesis of monodispersed nanocrystals in general.

ASSOCIATED CONTENT

Supporting Information. Detailed synthetic procedures, XRD spectra, additional TEM images, TGA data, and experimental setups. This material is available free of charge via the Internet at http://pubs.acs.org.

AUTHOR INFORMATION

Corresponding Author
cao@chem.ufl.edu

ACKNOWLEDGMENT

We thank Major Analytical Instrumentation Center (MAIC) at the University of Florida for TEM and XRD usage. Y.C.C.

acknowledges the NSF (DMR-0645520 Career Award), and the ONR (N00014-09-1-0441).

REFERENCES

(1) Carey, V. P. *Liquid-Vapor Phase-Change Phenomena*; 1st ed.; Taylor and Francis: New York, 1992.
(2) Dhir, V. K. *Annu. Rev. Fluid Mech.* **1998**, *30*, 365.
(3) Pavia, D. L. *Introduction to Organic Laboratory Techniques*; Thomson Brooks/Cole: Salt Lake City, UT, 2007.
(4) Yin, Y.; Alivisatos, A. *Nature* **2005**, *437*, 664.
(5) Peng, X. G.; Wickham, J.; Alivisatos, A. P. *J. Am. Chem. Soc.* **1998**, *120*, 5343.
(6) Murray, C. B.; Norris, D. J.; Bawendi, M. G. *J. Am. Chem. Soc.* **1993**, *115*, 8706.
(7) Cao, Y. C.; Wang, J. H. *J. Am. Chem. Soc.* **2004**, *126*, 14336.
(8) Yang, Y. A.; Wu, H. M.; Williams, K. R.; Cao, Y. C. *Angew. Chem., Int. Ed.* **2005**, *44*, 6712.
(9) Park, J.; An, K.; Hwang, Y.; Park, J.; Noh, H.; Kim, J.; Park, J.; Hwang, N.; Hyeon, T. *Nat. Mater.* **2004**, *3*, 891.
(10) Sun, S. H.; Murray, C. B.; Weller, D.; Folks, L.; Moser, A. *Science* **2000**, *287*, 1989.
(11) Cushing, B. L.; Kolesnichenko, V. L.; O'Connor, C. J. *Chem. Rev.* **2004**, *104*, 3893.
(12) Talapin, D. V.; Lee, J. S.; Kovalenko, M. V.; Shevchenko, E. V. *Chem. Rev.* **2010**, *110*, 389.
(13) Alivisatos, A. P. *J. Phys. Chem.* **1996**, *100*, 13226.
(14) Alivisatos, A. P. *Science* **1996**, *271*, 933.
(15) Pandey, A.; Guyot-Sionnest, P. *Science* **2008**, *322*, 929.
(16) Goldstein, A. N.; Echer, C. M.; Alivisatos, A. P. *Science* **1992**, *256*, 1425.
(17) Ozin, G. A. *Adv. Mater.* **1992**, *4*, 612.
(18) Jin, R. C.; Cao, Y. W.; Mirkin, C. A.; Kelly, K. L.; Schatz, G. C.; Zheng, J. G. *Science* **2001**, *294*, 1901.
(19) Casula, M. F.; Jun, Y. W.; Zaziski, D. J.; Chan, E. M.; Corrias, A.; Alivisatos, A. P. *J. Am. Chem. Soc.* **2006**, *128*, 1675.
(20) Liu, H. T.; Owen, J. S.; Alivisatos, A. P. *J. Am. Chem. Soc.* **2007**, *129*, 305.
(21) Kwon, S.; Piao, Y.; Park, J.; Angappane, S.; Jo, Y.; Hwang, N.; Park, J.; Hyeon, T. *J. Am. Chem. Soc.* **2007**, *129*, 12571.
(22) Lamer, V. K.; Dinegar, R. H. *J. Am. Chem. Soc.* **1950**, *72*, 4847.
(23) Mullin, J. W. *Crystallization*; 4th ed.; Reed Educational and Professional Publishing Ltd.: Oxford, 2001.
(24) *Crystallization Technology Handbook*; 2nd, Revised and Expanded ed.; Marcel Dekker, Inc.: New York and Basel, 2001.
(25) Xie, R. G.; Li, Z.; Peng, X. G. *J. Am. Chem. Soc.* **2009**, *131*, 15457.
(26) Sugimoto, T. *Monodispersed Particles*; 1st ed.; Elsevier: New York, 2001.
(27) Skinner, B. J. *Am. Mineral.* **1961**, *46*, 1399.
(28) Harris, D. C. *Quantitative Chemical Analysis*; 7th ed.; W. H. Freeman and Company: New York, 2007.
(29) Paula, P. A. a. J. d. *Physical Chemistry*; 7th ed.; W. H. Freeman: New York, 2001.
(30) Glasser, L. *Inorg. Chem.* **1995**, *34*, 4935.
(31) Davis, R.; Schultz, H. P. *J. Org. Chem.* **1962**, *27*, 854.
(32) Dollimor., D; Tonge, K. H. *J. Inorg. Nucl. Chem.* **1967**, *29*, 621.
(33) Kenfack, F.; Langbein, H. *Thermochim. Acta* **2005**, *426*, 61.
(34) Peng, Z. A.; Peng, X. G. *J. Am. Chem. Soc.* **2001**, *123*, 1389.
(35) Bronstein, L.; Huang, X.; Retrum, J.; Schmucker, A.; Pink, M.; Stein, B.; Dragnea, B. *Chem. Mater.* **2007**, *19*, 3624.
(36) Hyeon, T.; Lee, S. S.; Park, J.; Chung, Y.; Bin Na, H. *J. Am. Chem. Soc.* **2001**, *123*, 12798.
(37) Thome, J. R. *Enhanced Boiling Heat Transfer*; 1st ed.; Taylor and Francis: New York, 1990.
(38) Schmelzer, J. *Nucleation Theory and Applications*; Wiley-VCH: Weinheim, 2005.
(39) *CRC Handbook of Chemistry and Physics*; 91st ed.; Haynes, W. M., Ed.; CRC Press/Taylor and Francis: Boca Raton, FL, 2011.
(40) Fox, H. W.; Zisman, W. A. *J. Coll. Sci.* **1950**, *5*, 514.
(41) Chen, R.; Lu, M. C.; Srinivasan, V.; Wang, Z.; Cho, H. H.; Majumdar, A. *Nano Lett.* **2009**, *9*, 548.
(42) Kang, M. G. *Ann. Nucl. Eng.* **1998**, *25*, 295.
(43) *CRC Handbook of Chemistry and Physics*; 91st ed.; Haynes, W. M., Ed.; CRC Press/Taylor and Francis: Boca Raton, FL, 2011.
(44) Wechsler, B. A.; Lindsley, D. H.; Prewitt, C. T. *Am. Mineral.* **1984**, *69*, 754.
(45) Gatteschi, D.; Caneschi, A.; Pardi, L.; Sessoli, R. *Science* **1994**, *265*, 1054.
(46) Luo, Y. R. Bond Dissociation Energies in *CRC Handbook of Chemistry and Physics*; 91st ed.; Haynes, W. M., Ed.; CRC Press/Taylor and Francis: Boca Raton, 2011.
(47) van Embden, J.; Sader, J. E.; Davidson, M.; Mulvaney, P. *J. Phys. Chem. C* **2009**, *113*, 16342.
(48) Rempel, J. Y.; Bawendi, M. G.; Jensen, K. F. *J. Am. Chem. Soc.* **2009**, *131*, 4479.
(49) Robb, D. T.; Privman, V. *Langmuir* **2008**, *24*, 26.